PUBLISHED BY IOP PUBLISHING FOR SISSA

RECEIVED: *July 28, 2011*
ACCEPTED: *August 25, 2011*
PUBLISHED: *September 9, 2011*

13th INTERNATIONAL WORKSHOP ON RADIATION IMAGING DETECTORS,
3–7 JULY 2011,
ETH ZURICH, SWITZERLAND

In situ analysis of carrier lifetime and barrier capacitance variations in silicon during 1.5 MeV protons implantation

T. Ceponis,[a,1] **E. Gaubas,**[a] **V. Kalendra,**[a] **A. Uleckas,**[a] **J. Vaitkus,**[a] **K. Zilinskas,**[a] **V. Kovalevskij,**[b] **M. Gaspariunas**[b] **and V. Remeikis**[b]

[a] *Vilnius University, Institute of Applied Research, Sauletekio al. 9-III, LT-10222, Vilnius, Lithuania*
[b] *Centre for Physical Sciences and Technology, Savanoriu av. 231, LT-02300, Vilnius, Lithuania*

E-mail: tomas.ceponis@ff.stud.vu.lt

ABSTRACT: Results of the in situ measurements of the recombination lifetime and of barrier capacitance variations in Si substrates and pin diodes, respectively, during 1.5 MeV protons implantation are presented. Carrier recombination lifetime has been measured by employing microwave probed photoconductivity method, while parameters of the barrier capacitance changes have been extracted by transient technique of barrier capacitance charging current measurements using linearly increasing voltage pulses. Sub-linear decrease of carrier lifetime as a function of fluence has been revealed and peculiarities of such characteristic are explained in terms of formation of two layered structure within implanted Si material. Carrier recombination processes determine the increase of dielectric relaxation time within electrically neutral region (ENR) of a diode base. Carrier capture/emission processes within space charge (SC) and transition layer (between ENR and SC) regions lead to increase of generation/recombination currents in the irradiated diode.

KEYWORDS: Radiation damage evaluation methods; Interaction of radiation with matter; Detection of defects; Solid state detectors

[1] Corresponding author.

doi:10.1088/1748-0221/6/09/P09002

Contents

1 Introduction

Ion implantation technology is commonly employed for doping of shallow layers in formation of device structures [1, 2]. Ion implantation is also applied for the introduction of fast recombination centres in microelectronic devices [3]. Despite beneficial recombination centres, the detrimental defects that affect the device operation are introduced during implantation as well. Therefore, it is essential to analyze the characteristics of these defects. As usually, an analysis of the post-irradiated material is performed, which does not provide the direct information about processes of defects creation. Therefore, the in situ techniques, capable to reveal the peculiarities of defects creation during ion implantation, are desirable.

In this work, results of the in situ measurements of the carrier lifetime and of the barrier capacitance variations in Si substrates and pin diodes, respectively, during 1.5 MeV protons implantation are presented. The carrier recombination lifetime was measured by employing a microwave probed photoconductivity method (MW-PCD) by using optical-fibre excitation and coaxial needle-tip microwave probes inside the irradiation chamber. The parameters of the barrier capacitance changes in diode structures were extracted by a technique of barrier capacitance charging current measurements using the linearly increasing voltage pulses. The sub-linear decrease of carrier lifetime as a function of protons implantation fluence was revealed. Peculiarities of such characteristic are explained in terms of formation of two layered structure within the implanted Si material. Variations of the barrier capacitance in the pin diode structures during 1.5 MeV protons implantation indicated a decrease of the majority carriers within the electrically neutral region due to carrier capture by the radiation induced traps.

2 Samples and arrangement of experiments

High resistivity Si wafers of 300 μm thickness, containing the passivating SiO_2 layers on both surfaces, were investigated. Surface passivation ensures rather long effective carrier decay lifetime ($\tau_{\text{eff}} \geq 120\mu$s) with surface recombination velocity $s \leq$200 cm/s. Wafer fragments of dimensions of about 1×2 cm^2 were mounted on a cold finger within the irradiation chamber. Particle pad-detectors fabricated from high resistivity n-type Si were used for the measurements of barrier

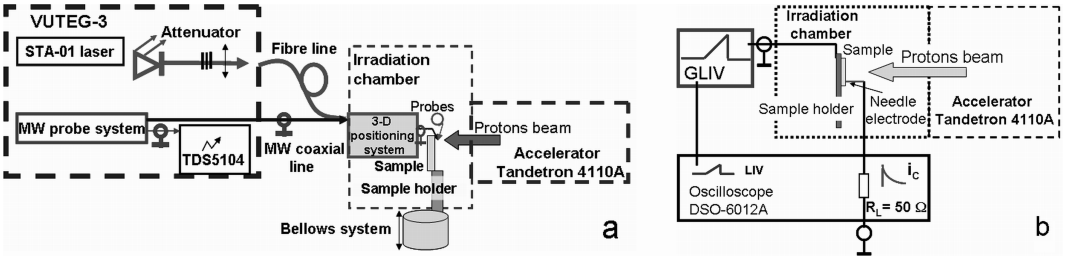

Figure 1. Sketches of the experimental setup for the in situ measurements of the microwave probed photoconductivity (a) and of the barrier capacitance charging current (b).

capacitance charging currents. The detectors with (p^+-n-n^+) diode structure had an active area of 5×5 mm^2. The thickness of the high resistivity base region of the pin diodes was about 300 μm, while the p^+ and n^+ layers are thinner (of 1–5μm thickness).

Sketches of the experimental setup for the in situ measurements of characteristics of the microwave probed photoconductivity (a) and of the barrier capacitance charging current (b) are shown in figure 1. The implantation of protons was performed by using the Tandetron 4110A ion accelerator. A beam current was changed in steps from 0.4 to 20 nA in order to vary more precisely the irradiation fluence. A protons flux was measured by using a Faraday-cup sensor.

A special irradiation chamber was designed and fabricated for these experiments. A cold finger with embedded sample is attached to the bottom component of the chamber, whose position can be adjusted by using bellow system and actuators, as can be seen in figure 1a. The single mode fibres were used to transfer of either 531 or 1062 nm excitation laser pulses to a sample within a vacuumed chamber, and a coaxial needle-tip microwave antenna was employed to register the photoconductivity response. Finally, the top component of the irradiation chamber contained the 3D steppers assisted positioning system for the location of the optical-fibre/microwave antennas onto the front-surface of wafer under irradiation. The excitation pulses with 100 Hz repetition rate and 400 ps duration were generated by a STA micro-chip laser [4]. Excitation wavelengths of 531 and 1062 nm were employed in sequence to separate carrier surface recombination rate and to evaluate carrier bulk lifetime, respectively [5–7]. The surface excitation wavelength of 531 nm was used to measure carrier decay rate within the protons projectile length and to profile the cross-sectional carrier lifetime distribution. The MW-PCD signal is collected by a coaxial needle-tip antenna which averages the excess carrier density variations within the output fibre-tip spot of dimensions of several microns. The averaged decay transients are measured every second and controlled by a PC.

For barrier capacitance charging current measurements, a pin diode was placed on a sample holder (attached to the bottom of the irradiation chamber) and connected the electrodes to the external measurement circuitry by a coaxial cable, as sketched in figure 1b. Current transients have been registered using the 50 Ω load input of the DSO6102A oscilloscope [8]. The measurement circuitry contains an adjusted output of a linearly increasing voltage generator (GLIV) and the diode under investigation, connected in series.

2011 JINST 6 P09002

3 Excess carrier decay and barrier capacitance charging current characteristics

The projectile depth of the 1.5 MeV protons within the Si wafers was about 30 μm nearby the front-surface of the sample under investigation, as obtained by simulations using the Transport of Recoils and Ions in Matter (TRIM) Monte Carlo simulation program [9]. Therefore, variations of carrier lifetime within protons beam irradiated volume were controlled by measurements of MW-PCD transients using surface excitation of 531 nm wavelength with effective excitation depth of $d_{\rm eff} = \alpha^{-1} + \sqrt{Dt}$. Here, α is the absorption coefficient at excitation wavelength, D the carrier diffusion coefficient, and t the time at which the carrier lifetime is controlled. Variations of the carrier density decay transients with protons irradiation exposure time are illustrated in figure 2a.

For the initial exposure irradiation segments, the excess carrier Δn decay transients are observed to be formed by two components, as can be seen from figure 2a. A significant and rapid decrease of the initial decay component is caused by a sharp excitation profile with short initial $d_{\rm eff}$ depth at 531 nm wavelength. The surface recombination component results from both lifetimes: $\tau_D = d_{\rm eff}^2/\pi^2 D$ related to the carrier diffusion towards the surface and $\tau_{s1} = d_{\rm eff}/s$ related to the surface recombination velocity s due to surface defects. The slope of the initial decay is determined by the non-linear depth-averaged carrier density decrease described as

$$\Delta n(t) = \Delta n(t=0) \sum_{m=1}^{\infty} A_m \exp\left(-t \left[\tau_b^{-1} + \tau_{\rm sm}^{-1} \right] \right) \tag{3.1}$$

for observation time t over a system of distributed parameters within the surface ($\tau_{\rm sm}$) and the bulk (τ_b) of the sample of thickness d. This carrier density reduction rate is controlled by the amplitudes (A_m) associated with every spatial m-mode η_m [5–7]. The asymptotic stage of carrier density relaxation is characterized by the exponential decay with an effective lifetime $\tau_{\rm eff} = 1/\tau_b^{-1} + 1/(\tau_{s1} + \tau_D)]$, ascribed to the main decay mode. The control of the the carrier decay transient shape allows resolving the fluence (exposure duration) values for which recombination within the surface layer becomes prevailing. Afterwards the carrier density relaxation transient becomes single-exponential, and the decay slope can be exploited to directly extract the carrier lifetime ($\tau_{\rm Rs}$) associated with the radiation induced defects density within the implanted layer bulk. In order to extract the bulk and the surface recombination parameters, the changes of $\tau_{\rm eff}$ and of A_1 with varying excitation depth have been measured between irradiations, when protons beam is switched off.

The difference between carrier lifetimes within the implanted layer and the non-irradiated bulk was verified by combining measurements with different excitation wavelengths and carrier lifetime depth-profiling. The evaluated carrier decay lifetime $\tau_{\rm Rs}$ as a function of depth coordinate (x) within the wafer sample boundary (along the wafer thickness direction) is plotted in figure 2b. The narrow range of the shortest carrier decay lifetimes $\tau_{\rm Rs}$ is observed at the expected position of $R \leq 30\mu$m within $\tau_{\rm Rs}(x)$ of the profile. The values of $\tau_{\rm Rs}(x)$ are enhanced relatively to those at front-surface, and stabilized far behind R, being rather constant across the non-irradiated material. It was possible to deduce from two-componential transients and from the amplitude analysis of the asymptotic decay constituent, that a two-layered structure is formed under implantation. The transformation of the transient into a single exponential decay shows that the bulk recombination within the front implanted layer prevails. Values of $\tau_{\rm Rs}$ and their depth-distribution correctly represent the $\tau_{\rm Rs}(x)$ profile.

2011 JINST 6 P09002

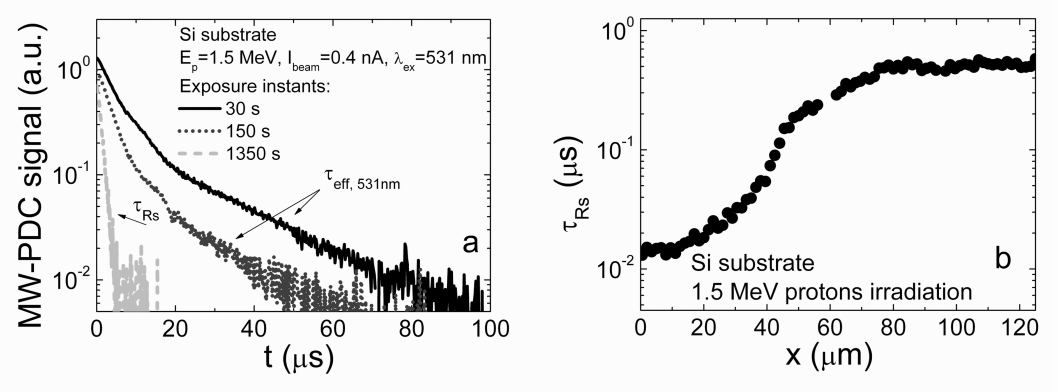

Figure 2. (a) Variations of carrier decay transients versus protons irradiation exposure time. (b) Distribution profile of the carrier decay lifetime (τ_{Rs}) within Si wafer cross-sectional boundary measured after 1.5 MeV protons implantation.

These profiling results corroborate the fluence dependent variations of τ_{Rs} measured in situ, shown in figure 3, as a function of exposure duration (bottom scale) and fluence (top scale). It can be noticed in figure 3 that the slower reduction of τ_{Rs} with enhancement of irradiation fluence is obtained within the initial exposure episodes ($t_{exp} < 10$ s). The sub-linear reduction of $\tau_{Rs} \sim \Phi^{-1/2}$ was obtained as a function of the fluence enhancement within a wide range (t_{exp} = 10–20000 s) of exposure times. The obtained fluence dependent variations of $\tau_{Rs} \sim \Phi^{-1/2}$ within the protons projectile range can be explained by the increase of the radiation defects density, which determines a reduction of distances (l_d) among defects. Due to a sharp recombination boundary at the projectile range of protons and due to beam induced lateral inhomogeneity of defects density, the carriers experience two-directional gradients within the implanted layer. On the basis of the mentioned assumptions, the proportionality relations are derived, as $\tau_{Rs} \sim 1/N \sim l_d^2 \sim \Phi^{-1/2}$ when the introduction rate of the dominant radiation defects varies linearly with fluence.

In diode structures, carrier recombination processes determine the dielectric relaxation time within the electrically neutral region (ENR) of a diode and the stabilization time scale of the depletion width. On the other hand, carrier capture/emission processes within the space charge (SC) and the transition layer (between ENR and SC) regions impact the diode generation/recombination currents. Therefore, correlation between the in situ variations of the carrier lifetime, measured by MW-PCD technique in wafer samples, and of the barrier capacitance charging current transients examined in diodes fabricated on the same Si material, is essential.

The evolution of the barrier capacitance charging current transients with irradiation exposure time, measured by using the reverse bias linearly increasing voltage pulses, is illustrated in figure 4.

The technique of barrier evaluation by linearly increasing voltage (BELIV) [10], using a reverse biased diode, is based on the analysis of the barrier capacitance (C_b) changes with the linear increase of the voltage $U = At$ pulse. The $C_b(t)$ dependence on voltage and on time t can be described using the depletion approximation [11] for charge extraction from the diode base region. This approximation leads to a simple relation $C_b = C_{b0}(1 + U/U_{bi})^{-1/2}$ for an abrupt p^+-n junction, where the barrier capacitance for a non-biased diode of an area S is $C_{b0} = \varepsilon\varepsilon_0 S/w_0 = (\varepsilon\varepsilon_0 S^2 e N_D/2U_{bi})^{1/2}$. Here ε_0 is the vacuum permittivity, ε the material dielectric permittivity, e

2011 JINST 6 P09002

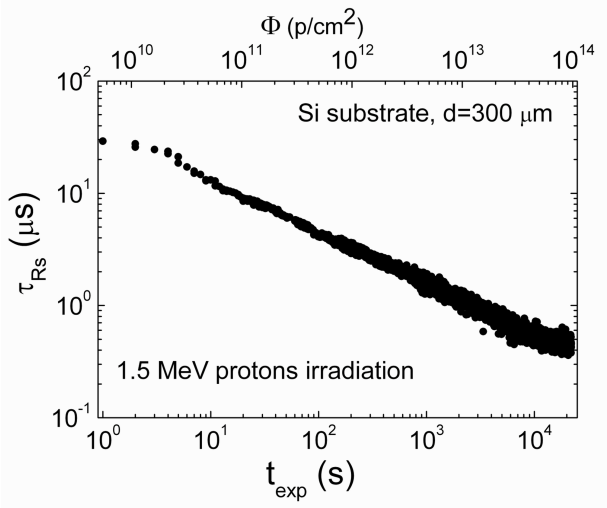

Figure 3. Carrier decay lifetime τ_{Rs} measured within the implanted Si wafer layer as a function of both the exposure time (bottom scale) and 1.5 MeV protons fluence (top scale).

the elementary charge, U_{bi} the built-in potential barrier, $w_0 = (2\varepsilon\varepsilon_0 U_{\mathrm{bi}}/eN_D)^{1/2}$ the depletion width for the non-biased junction, $A = U_P/\tau_{\mathrm{PL}}$ the ramp of LIV pulse of U_P amplitude and of τ_{PL} duration of the LIV pulse. The depletion approximation [11] is acceptable to describe the charge extraction transients in the time scale t longer than that of the dielectric relaxation $\tau_M = \varepsilon\varepsilon_0/e\mu N_D$. This is maintained by a short Debye length $L_D = (2\varepsilon\varepsilon_0 kT/e^2 N_D)^{1/2}$ relatively to the characteristic depletion widths w_0, $w = w_0(1+U/U_{\mathrm{bi}})^{1/2}$, and of a geometric thickness d ($L_D \ll w_0$, w, d). The time dependent changes of charge $q = C_b U$ within junction determine a current transient $i_C(t)$ in the external circuit:

$$i_C(t) = \frac{dq}{dt} = \frac{\partial U}{\partial t}\left(C_b + U\frac{\partial C_b}{\partial U}\right) = AC_{b0}\frac{1+\frac{At}{2U_{\mathrm{bi}}}}{\left(1+\frac{At}{U_{\mathrm{bi}}}\right)^{3/2}}. \tag{3.2}$$

This transient contains an initial ($t = 0$) step AC_{b0} due to the displacement current and a descending constituent governed by charge extraction. In reality, a delay appears due to the serial processes of dielectric relaxation within the quasi-neutral range of the non-depleted n-layer, the drift and diffusion of the carriers to complete the circuit. The characteristic delay lifetimes are summarized as τ_{RC}. In materials containing a considerable density of deep traps, the modification of the $i_C(t)$ current transient is governed by carrier capture/release processes. These traps are responsible for the generation current within the depletion region. The generation current $i_g(t) = en_i w_0(1+At/U_{\mathrm{bi}})^{1/2}/\tau_g$ increases with voltage $U(t)$ and can exceed the barrier charging current in the rearward range of pulsed current transient when the carrier generation lifetime τ_g is rather short. In this case the transient of the total reverse current is described by the sum of the currents:

$$i_{R\Sigma}(t) = i_C(t) + i_g(t) = AC_{b0}\frac{1+\frac{At}{2U_{\mathrm{bi}}}}{\left(1+\frac{At}{U_{\mathrm{bi}}}\right)^{3/2}} + \frac{en_i S w_0}{\tau_g}\left(1+\frac{At}{U_{\mathrm{bi}}}\right)^{1/2}. \tag{3.3}$$

The descending charge extraction and ascending generation current variation with LIV pulse time

2011 JINST 6 P09002

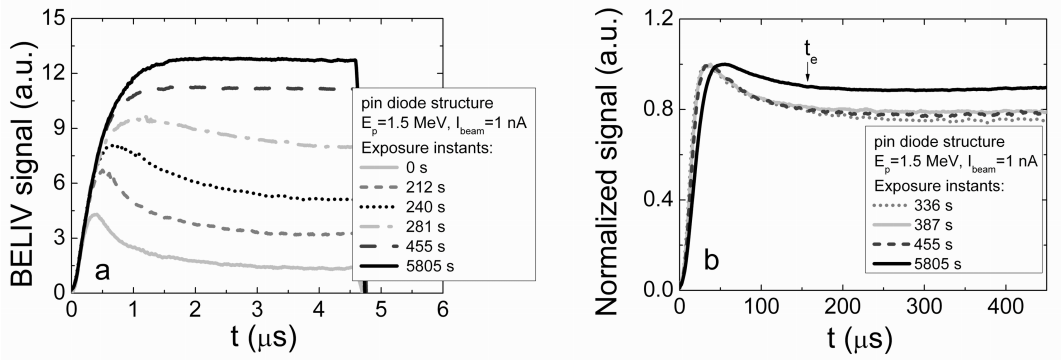

Figure 4. Variation of barrier capacitance charging current transients with irradiation exposure time (denoted within legends), measured using reverse bias linearly increasing voltage pulses of duration: $\tau_{\mathrm{PL}} = 4.5\mu$s (a) and $\tau_{\mathrm{PL}} = 450\mu$s (b), respectively.

(voltage) implies the existence of a current minimum within the transient, characterized by the time instant t_e.

On the above mentioned basics in describing the barrier charging current transients, the evolution of these transients with irradiation exposure time can be explained by simultaneous increase of the SC generation current, of the dielectric relaxation time and of the consequent enhancement of series resistance within diode base region, as can be seen in figure 4. For the very initial irradiation stages, the typical barrier capacitance charging current ($i_C(t)$) transients are observed (figure 4a) for rather short (4.5 μs) LIV pulses. These transients indicate rather fast dielectric relaxation processes with $\tau_M \ll \tau_{\mathrm{PL}}$. An increase of the irradiation exposure time leads to the enhancement of the SC generation current and to the increase of the total current, observed as the increment of the BELIV signal amplitude in figure 4a. For rather short LIV pulses this amplitude saturates, as τ_{RC} is increased, due to enhanced series resistance within ENR, as the density of equilibrium carriers rapidly falls down through recombination, when the density of radiation induced defects increases with fluence. This also leads to an elongation of τ_M. Therefore the typical transients of barrier charging currents can be observed only when the duration of the LIV pulses is significantly increased (figure 4b). The SC generation current also increases and it is observed as an increment of the BELIV signal amplitude. The prevailing of SC generation current over barrier capacitance charging current can be resolved for LIV pulses in the time scale of $\tau_{\mathrm{PL}} = 450\mu$s (figure 4b). Then, the time instant, for which total current minimum ($t_e \cong 150$ μs) is reached, can be separated.

The observed decrement of carrier recombination lifetime, revealed by MW-PCD measurements, leads to a reduction of equilibrium carrier density within ENR and to an increase of generation current, due to emission of these captured carriers within SC region. So, the results of these in situ measurements of the MW-PCD and BELIV characteristics correlate well, when comparing the controlled characteristics as a function of irradiation fluence.

4 Summary

The applied MW-PCD technique for the in situ analysis of recombination parameters during implantation of 1.5 MeV protons enabled us to control the production of radiation induced defects

2011 JINST 6 P09002

and the evolution of their density with fluence. The sub-linear decrease of carrier recombination lifetime $\tau_{Rs} \sim \Phi^{-1/2}$ as a function of fluence was revealed in wafer samples. Peculiarities of this irradiation characteristic are explained by the formation of a two-layered structure of the implanted silicon wafer. Carrier recombination processes determine the increase of dielectric relaxation time within electrically neutral region (ENR) of a diode base. This leads to the elongated time scale of stabilization of depletion width. Carrier capture/emission processes within space charge (SC) and transition layer (between ENR and SC) regions lead to an increase of generation/recombination currents in the irradiated diode.

Acknowledgments

E. Tuominen and J. Harkonen are appreciated for providing the samples. This work has been supported by the Research Council of Lithuania, grant MIP-11018.

References

[1] V. Kozlovski and V. Abrosimova, *Radiation defect engineering*, World Scientific, Singapore, (2005).

[2] M. Nastasi and J.V. Mayer, *Ion implantation and synthesis of materials*, Springer, U.S.A. (2006).

[3] P. Hazdra and V. Komarnitskyy, *Lifetime control in silicon power P-i-N diode by ion irradiation: suppression of undesired leakage*, *Microelectr. J.* **37** (2006) 197.

[4] *Standa, Opto-Mechanical Products*, http://www.standa.lt/products/catalog/lasers_laser_accessories.

[5] E. Gaubas, *Transient absorption techniques for investigation of recombination properties in semiconductor materials*, *Lith. Journ. Phys.* **43** (2003) 145.

[6] E. Gaubas, J. Vaitkus, E. Simoen, C. Claeys and J. Vanhellemont, *Excess carrier cross-sectional profiling technique for determination of the surface recombination velocity*, *Mat. Sci. Semicon. Proc.* **4** (2001) 125.

[7] E. Gaubas and J. Vanhellemont, *A simple technique for the separation of bulk and surface recombination parameters in silicon*, *J. Appl. Phys.* **80** (1996) 6293.

[8] *Agilent Technologies*, http://www.home.agilent.com/agilent.

[9] *Particle interactions with matter*, http://www.srim.org.

[10] E. Gaubas, T. Ceponis and J. Vaitkus, *Impact of generation current on the evaluation of the depletion width in heavily irradiated Si detectors*, *J. Appl. Phys.* **110** (2011) 033719.

[11] P. Blood and J.W. Orton, *The electrical characterization of semiconductors: majority carriers and electron states*, Academic Press, U.S.A. (1992).

2011 JINST 6 P09002